



Observational and Numerical Methods for Quantifying and Modeling of Turbulence in a Stratified Reservoir

S. Elçi[†] and B. Ekmekçi

Department of Civil Engineering, Izmir Institute of Technology, Izmir, Turkey,

[†]Corresponding Author Email: sebnemelci@iyte.edu.tr

(Received May 25, 2015; accepted August, 23, 2015)

ABSTRACT

The interplay between stratification and shear in lakes controls the vertical mixing, which is the most important mechanism affecting the transport of heat, salt, momentum and suspended and dissolved substances. This study attempts to quantify and characterize the turbulence from direct measurements conducted in a reservoir. A 3D numerical model is used to investigate the water column hydrodynamics for the duration of measurements and the performance of various turbulence models used in the CFD model are investigated via simulation of mixing in the reservoir. The drawdown curves produced by the turbulence models are formulized through linear equations. Although, use of different turbulence models do not have significant effects on the flow hydrodynamics away from the intake structure; significant effects especially on turbulence kinetic energy production are observed at the orifice. Therefore, for simulation of withdrawal flow, either use of shear stress transport (SST) k-omega models solving equations all the way to the wall or k-epsilon models with the nonequilibrium wall function is recommended to account for the changes in the pressure gradient. In this study, the methods using quantified turbulent characteristics of the flow to reformulate the Stokes' settling velocity to be applied in turbulent flows are also investigated. An approach to predict setting velocity in turbulent flows that utilizes acoustic Doppler instruments for quantification of turbulent characteristics is presented. Modification of the Stokes' settling velocity with the nondimensionalized turbulent kinetic energy production profiles lead better results than other turbulence characteristics (buoyancy flux and by Richardson number flux) widely used in characterizing turbulent mixing.

Keywords: Vertical mixing; Stratified reservoirs; Turbulent mixing; Turbulence models; Settling velocities.

NOMENCLATURE

B	buoyancy flux	T	water temperature
Fr_t	turbulence Froude number	T'	fluctuations of water temperature
Fr_γ	strain ratio	u	longitudinal velocity
g	gravity	u'	fluctuations of longitudinal velocity
L_t	turbulent length scale	w	vertical velocity
N	buoyancy frequency	w'	fluctuations of vertical velocity
P	turbulent kinetic energy production	z	depth
q	turbulent kinetic energy	ε	dissipation of turbulent kinetic energy
Re_t	turbulence Reynolds number	ρ	water density
Ri	Richardson number	ρ_0	reference water density
R_f	Richardson number flux	ρ_s	sediment density
S	Reynolds-averaged vertical shear	Ω	stokes' settling velocity
		ν	molecular viscosity

1. INTRODUCTION

Turbulence in a stratified reservoir in general is

produced by mean shear due to changes in kinetic energy generated by winds or tides and by unstable stratification due to changes in potential energy.

Advancements in measurement technology resulted in availability of higher frequency acoustic Doppler current profilers (ADCP) enabling estimation of turbulence parameters.

Research on understanding of turbulent-mixing in stratified lakes available in the literature include analytical, numerical, and field studies (mainly in oceans and lakes) (Stacey *et al.* 1999, Etemad-Shahidi and Imberger, 2001, Saggio and Imberger, 2001, Geyer *et al.* 2008 and Burchard *et al.* 2008). In these studies, observations were in general conducted with high resolution profiling instruments measuring velocities and temperature from which density can be inferred simultaneously. Turbulence characteristics were studied by several researchers in the past, although none related these characteristics to the settling velocity. Of these studies, the paper by Etemad-Shahidi and Imberger (2001) and Saggio and Imberger (2001) investigated anatomy of turbulence in stratified lakes. The first authors used a portable flux profiler to measure high resolution profiles of temperature, conductivity and two components of velocity in two stratified lakes in Japan (Lake Biwa) and in Israel (Lake Kinneret). In parallel with this study, Saggio and Imberger (2001) evaluated high resolution velocity and temperature measurements conducted in Lake Kinneret and presented an approach for separation of turbulence fluctuations from the measured signals. Both studies indicated that, *the turbulence Froude number* ($Fr_t = \sqrt{q}/(L_T \times N)$), *the turbulence Reynolds number* ($Re_t = (\sqrt{q} \times L_T)/\nu$) and *the strain ratio* ($Fr_\gamma = \sqrt{\varepsilon}/(\nu \times N^2)$) were found especially effective parameters to characterize turbulence in the thermocline.

Where (q) is the turbulent kinetic energy, (L_T) is the turbulence scale, (N) is the buoyancy frequency, (ν) is the molecular viscosity, and (ε) is the dissipation of turbulent kinetic energy.

Etemad-Shahidi and Imberger (2001) observed that turbulence in the thermocline had intermittent but dissipative character. Most of the turbulent segments exhibited low values of the turbulence Froude number resulting in a very low net mixing efficiency. Saggio and Imberger (2001) also observed that turbulent events had higher dissipation levels than found in the oceanic thermocline, where dissipation was estimated as $3 \times 10^{-7} \text{ m}^2\text{s}^{-3}$. High dissipation levels with small overturn scales (length scale of turbulence growth/decay) produced a wide range of turbulent Reynolds numbers (Re_t). Their study also showed that turbulent kinetic energy (q) is directly related to the rate of dissipation of turbulent kinetic energy (ε_B) estimated as a function of temperature gradient and to the turbulence scale (L_T) with the following equation:

$$\sqrt{q} = 1.3 \times (\varepsilon_B L_T)^{1/3} \quad (1)$$

Richardson number was related with the strain ratio for the period of sampling as follows

$$Fr_\gamma = 2.3 / Ri^{3/4} \quad (2)$$

Where Richardson number, Ri , is a measure of the interaction of Reynolds stresses with the shear and the stratification and its formulation is given below. For values of $Ri < 0.25$ the mean shear flow is relatively strong as compared with stratification to produce turbulence (Stacey *et al.* 1999, Burchard *et al.* 2008).

$$Ri = -\frac{g}{\rho} \frac{\partial \rho}{\partial z} \frac{1}{\left(\frac{\partial w}{\partial z}\right)^2} \quad (3)$$

where (g) is the gravity, (ρ) is the density, (z) is the depth and (w) is the vertical velocity.

Difficulties in specification of the vertical mixing in stratified reservoirs motivated the researchers to characterize the turbulent mixing by various parameters. Ivey *et al.* (2008) pointed out the fundamental problem as highly unsteady and inhomogeneous character of the vertical component of the mixing that is influenced by the gravitation. They also blamed the vertical component for potential interpretation problems. Also the variability of turbulence intensities and the transition of flow from laminar to turbulent regime and back again results were presented as interpretation problems. Ivey *et al.* (2008) suggested based on numerical model simulations presented by Shih *et al.* (2005), there exists three regimes in mixing: a molecular regime, a transitional regime and a fully energetic regime. The square of the strain ratio is the determiner for the regimes and for values of $Fr_\gamma^2 < 7$ molecular and for values of $Fr_\gamma^2 > 100$ fully energetic regimes are observed respectively.

Geyer *et al.* (2008) discussed approaches to quantify mixing in estuaries. Data monitored at various estuaries having high values of both dissipation rate (ε) and buoyancy frequency (N) lead to a distinct subrange in velocity and salinity spectra that was utilized to quantify turbulence quantities. They searched for relationship between turbulence dissipation rate and buoyancy frequency and compared the conditions in estuaries, lakes and oceans on a plot of dissipation rate versus buoyancy frequency. Based on the plot they pointed out that active turbulence cannot be maintained when ($\varepsilon/\nu N^2 < 20$).

Literature review on the topic revealed that the turbulence models tend to underestimate the turbulent kinetic energy in regions of strong stratification and overestimate it in regions of weakly stratified regions. In many cases, researchers pointed out the difficulty in characterizing turbulent mixing in stratified conditions. Also literature review indicated that

none of the researchers discussed the possibility of reformulating the Stokes' settling velocity for the turbulent flow. This study aims to investigate the application of acoustic Doppler instruments for reformulation of settling velocity for turbulent flow conditions. This study also presents a thorough discussion of different turbulence models used for water withdrawal. For this purpose field data monitored in front of a water withdrawal structure of a stratified reservoir is utilized.

2. METHODS

2.1 Analysis of Observed Data

The mixing efficiency, ratio of the rate at which the buoyancy forces extract energy from turbulence to the rate of energy available for mixing is vital in parameterizing small-scale mixing processes. It is dependent on Richardson number flux that is calculated as a ratio of buoyancy flux to the summation of buoyancy flux and dissipation:

$$R_f = \frac{B}{B + \varepsilon} = \frac{g}{\rho_0} \overline{w' \rho'} \left/ \left(\frac{g}{\rho_0} \overline{w' \rho'} + \nu \frac{\partial u'}{\partial z} \frac{\partial u'}{\partial z} \right) \right. \quad (4)$$

where w' and u' are the fluctuations of the vertical and horizontal velocities and water density is calculated as function of instant temperatures (given in °C) using the formulation below (McCutcheon *et al.* 1993):

$$\rho = 1000 \times \left[1 - \left(\frac{T + 288.94}{508929.2 \times (T + 68.13)} \right) \times (T - 3.986)^2 \right] \quad (5)$$

Similarly values of water viscosity is calculated using equation 6:

$$\nu = \frac{1.775 \times 10^{-6}}{1 + 0.0337T + 0.000221T^2} \quad (6)$$

Based on the fluctuations of the vertical velocities and temperatures buoyancy flux is calculated.

$$B = \frac{\partial \rho}{\partial z} \frac{1}{\rho} \overline{g T' w'} \quad (7)$$

where T' is the fluctuation of water temperature. Turbulent kinetic energy production, P, is related to $\overline{u' w'}$ (Reynolds stress) representing the vertical transport of momentum by turbulence and $\overline{\partial u' / \partial z}$ (Reynolds-averaged vertical shear, S) which can be derived from the measurements for the selected time interval and cell depth in the vertical.

$$P = -\overline{u' w'} \frac{\partial \overline{u'}}{\partial z} = \overline{u' w'} S \quad (8)$$

2.2 Reformulation of the Settling Velocity Based on Observed Data

In the literature, settling velocities in turbulent flow are estimated based on the Stokes' settling velocity (Ω) defined for the laminar flow in 1851. Stokes' theory states that when the particles are falling in

the viscous fluid by their weight, the settling (terminal) velocity is reached when frictional and buoyant forces balance the gravitational force (Yang, 1996).

$$\Omega = \frac{1}{18} \frac{\rho_s - \rho}{\rho} \frac{g d^2}{\nu} \quad (9)$$

where ρ_s is the density of sediment and d is the particle diameter.

To utilize Stokes' equation, the flow must be experiencing negligible turbulence, which is not the case in most flows. Also, it is assumed that viscous forces dominate the flow and pressure drag based on vertical velocities is neglected. Since these assumptions are not valid in most cases, application of the Stokes' settling velocity results in considerable errors especially in modeling studies. In this study, we investigate the methods that use quantified turbulent characteristics of the flow to reformulate the Stokes' settling velocity to be used in turbulent flows. Within this scope, turbulence characteristics are characterized by buoyancy flux and by Richardson number flux which consider the fluctuations of the vertical (w') and horizontal velocities (u') and the fluctuations of the density (ρ') in their formulation. Modified settling velocities are compared with the z component of velocity measurements performed by ADCP in Tahtali Reservoir. An ADCP operates by transmitting "pings" of sound at a constant frequency into the water. As the sound waves travel, they hit the particles suspended in the moving water, and are reflected back to the instrument. The difference in frequency between the waves sent out and received by the profiler is called the Doppler shift. An ADCP uses this shift to calculate how fast the particle and the water around it are moving. In this study, settling velocities of the particles are assumed to be equal to the vertical velocities of the flow measured by the ADCP.

2.3 CFD Modeling of the Flow

CFD modeling applied to surface water reservoirs involves solving the Reynolds-averaged Navier–Stokes equations describing the flux of mass and momentum within a fixed domain and subject to specified boundary conditions. The fate and transport of substances within the system are modeled with equations describing discrete particle trajectories.

In the present study, a 3D CFD model (FLUENT) is applied to the Tahtali Reservoir to determine the effects of different turbulence modeling approaches on predicted velocities and turbulence characteristics of a stratified reservoir. The use of the model to simulate the hydrodynamics in modeled portion of Tahtali Reservoir included the following tasks:

- i. Construction of the model (generation of appropriate geometric mesh, selection of appropriate initial and boundary conditions).
- ii. Solution of flow equations

- iii. Simulation of flow velocities and turbulence kinetic energy for different turbulent models
- iv. Selection of the appropriate turbulent model and discussion of results.

Solution of Navier-Stokes Equations for the mean flow are derived by Reynolds decomposition into instantaneous equations and applying time averaging. Reynolds averaged Navier-Stokes Equations have new unknowns to be solved, thus fluctuating velocity components need to be modeled by turbulence modeling strategies for closure. Of the available turbulence models in FLUENT, $k-\epsilon$; $k-\omega$ and Reynolds Stress turbulence models are used in the simulations and the results of these models will be discussed in the coming sections. Two equation models ($k-\epsilon$; $k-\omega$) are the simplest complete turbulence models used to predict turbulent flow without prior input about the structure of it. They employ two additional partial differential equations (one for the velocity and one for the length scale) to calculate the turbulence velocities. The same transport equation is employed for the turbulent kinetic energy (TKE) to calculate a local turbulence velocity. In $k-\epsilon$ models, the actual rate of dissipation, (ϵ) is utilized whereas the specific dissipation rate that is dissipation per unit kinetic energy, ($\omega = \epsilon/k$) is employed in the $k-\omega$ model (FLUENT 2014). The $k-\epsilon$ equations are valid only far from solid boundaries. There are three primary impacts of the wall on the structure of turbulence: 1) turbulent eddies are distorted and constrained in size, 2) production of turbulence increases due to no-slip condition, 3) turbulence energy is damped and dissipated into heat via viscous action. Thus the model equations become ill-conditioned close to the wall. To avoid this problem, common approach is adopting wall functions. Standard wall functions; nonequilibrium wall functions, enhanced wall treatment (two-layer zonal model) and user defined functions are the available options for wall treatment in the FLUENT model (FLUENT 2014). The $k-\omega$ model at the other hand is designed to be applied throughout the boundary layer when a sufficiently fine mesh is available. The $k-\omega$ equations are well posed inside the laminar sublayer and the model equations can be integrated all the way to wall.

In standard wall functions, the near wall flow is assumed to be dependent on local variables and near wall velocity profile is considered. The computational grid is constructed such that the first grid point which is not located on the wall is located within the fully turbulent region. Boundary conditions are then applied assuming the mean velocity field as logarithmic, and an equilibrium between turbulence production and energy dissipation is implemented to specify boundary conditions for k and ϵ . In nonequilibrium wall functions, logarithmic velocity profile for mean velocity is modified to include pressure gradient enabling better prediction of adverse pressure gradient flows and separation. In two layer zonal model, the flow domain is divided into two: the inner layer covering the sublayer, the buffer layer and portion of the turbulent region and the outer

layer. In the inner layer, only the k -equation is solved and the ϵ equation is replaced by an algebraic equation that considers the viscosity of the fluid and the turbulence length scale. These models are more robust than standard $k-\epsilon$ models (FLUENT 2014).

Reynolds Stress turbulence models utilize transport equations for the individual Reynolds stresses and are only valid within the fully turbulent region. Likewise $k-\epsilon$ turbulence models, the equations are modified to account for near wall effects. In FLUENT, three wall functions: standard wall functions; nonequilibrium wall functions and enhanced wall treatment are available options for wall treatment. For standard and nonequilibrium wall functions, Reynolds stresses at the wall-adjacent cells are computed from the equations whereas FLUENT applies zero flux wall boundary conditions to the Reynolds stress equations when using enhanced wall as the near-wall treatment (FLUENT 2014). The discussion on different wall treatment functions are provided within the comparison of turbulence models section.

3. FIELD DATA MONITORING

The observations were conducted in Tahtali Reservoir, Menderes, Turkey to monitor synchronized velocity and temperature time series data, and sediment data. Tahtali Dam was constructed as a rockfill dam and completed in 1996 to supply fresh water to the city of Izmir, the third largest metropolitan area with over 3 million population. The capacity of the dam is 175 million m^3 and it generates monthly 5 million m^3 water. The dam is currently operated by IZSU (Izmir Water and Sewage Administration) (Çalışkan and Elçi 2009).

Tahtali Reservoir has a surface area of 20 km^2 , a mean depth of 15 m, with a maximum depth of 27 m. The major inflows are from North via Sasal Stream and Tahtali Stream. Sasal Stream contributes 25% whereas Tahtali Stream contributes 75% to the total inflow. The discharges of the other four streams are negligible. The withdrawal point is at southwest location of the lake from the deepest area corresponding to 27 m. The water is provided as drinking water for the city of Izmir after being treated. The retention time of the reservoir is 2.5 years calculated based on volume of the lake and outflow rate. The lake begins to stratify thermally in April and mixing in the water column is observed by the end of September. Water is generally withdrawn from hypolimnetic outlets with an average flow rate of 3 m^3/s . The site is exposed to the full force of wind blowing mostly from East as well as from North. The average annual wind speed is 3 m/s. The local has a Mediterranean climate, with average annual temperatures for the warmest month July at 28°C and for the coldest month January at 8°C.

Simulations presented in this paper are conducted based on measurements made in the Tahtali Reservoir on June 6th, 2013 (Figure 1). During the

measurements, wind speed was constant at 3.3 m/s. Air temperature was 26 °C and water was withdrawn from the first outlet at a rate of 2.9 m³/s that is positioned 9.00 m below the water surface (50 m above sea level). Water density was defined based on the measured temperature profile as shown in Figure 2. As can be inferred from the figure,

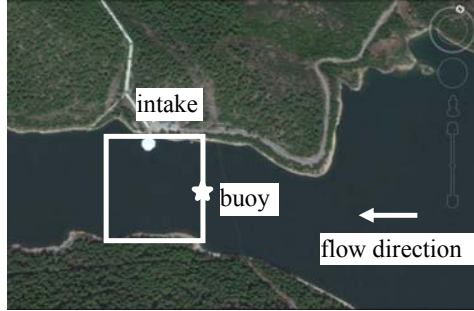


Fig. 1. Plan view of the study site.

water column has begun to stratify at the time of measurements and the surface temperature reached to 22 °C whereas bottom temperatures were as low as 15.6 °C.

The aim of the deployment was to collect synchronized 3-D velocity and temperature time series data and for this purpose a 1.5 MHz Acoustic Doppler current Profiler (ADCP-River Cat) was mounted to a buoy in down-looking mode (Figure 3) with an accuracy of 0.25% of measured velocity, resolution of 1mm/s. The sampling frequency was set to 1 second to have synchronized measurements with the thermistors. Blanking distance of the ADCP was defined as 62.5 cm, so that velocity measurements in the vertical were recorded at the same locations with the temperature measurements recorded by the sensors of the thermistor chain. Vertical resolution of both velocity and temperature measurements were 25 cm. The measurements extended for 40 cells corresponding to 10 m of depth. A thermistor chain having 16 thermistors placed 25 cm apart on a cable was used and mounted on the same buoy. The thermistor chain and the ADCP were lined up so that the depth of the readings obtained from the first thermistor corresponded to the velocity readings monitored by the ADCP at the 22nd cell and the readings obtained from the last thermistor corresponded to the 38th cell as shown in Figure 4.

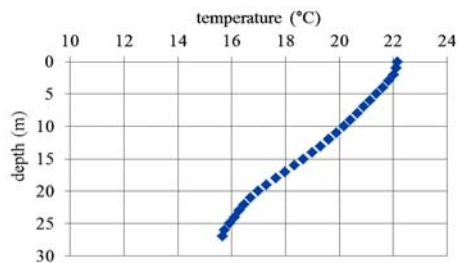


Fig. 2. Temperature values measured along the water column during field measurements.



Fig. 3. ADCP and thermistor chain mounted to a buoy to monitor synchronized velocity and temperature data.

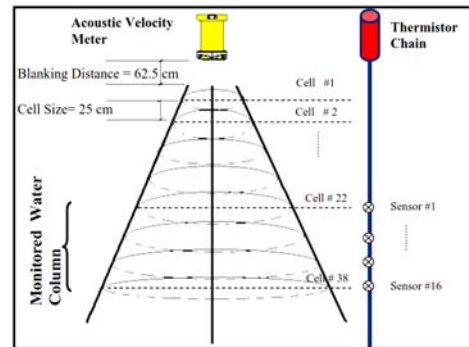


Fig. 4. Schematization of ADCP and thermistor chain used to monitor synchronized velocity and temperature data throughout the water column.

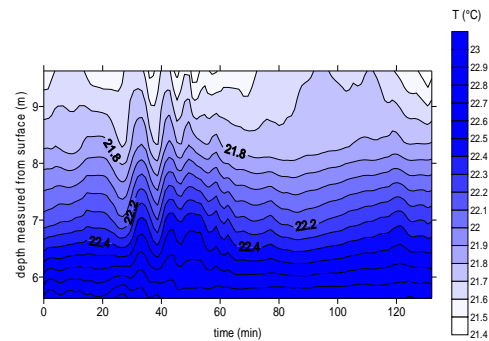


Fig. 5. Temperature measurements recorded by the thermistors during the deployment.

Thermistors deployed for this study are produced by Ruskin and have accuracy of $\pm 0.002^\circ\text{C}$. Sampling was made at 1 second frequency. Temperatures varied between the maximum of 15.2 °C recorded by the top thermistor to the minimum of 11 °C recorded by the bottom thermistor during the first deployment. The difference of the top and bottom thermistors' temperatures reached to 1.6 °C (Figure 5). Average velocities were 0.016 m/s, 0.013 m/s and 0.005 m/s for long-shore, cross-shore and upward velocities respectively.

4. CHARACTERIZATION OF TURBULENCE AND MIXING EFFICIENCY

Following the literature, the turbulence characteristics were characterized by Richardson number and buoyancy fluxes. Since these formulations involve the fluctuations of the vertical (w') and horizontal velocities (u') and the fluctuations of the density (ρ') by definition, these quantities are calculated by subtracting 1 minute averaged values from the instantaneous measurements.

The relative strengths of stratification and shear are assessed by the Richardson number flux, R_f , as defined by Equation 4 and 1 minute averaged values of R_f are plotted in Figure 6 (a). The resultant R_f values are above the critical limits defined by the other researchers (0.25) and one would expect less mixing in these zones. In fact, since most of the calculated values of R_f values are above the critical limits, it was presumed that turbulent mixing is strongly inhibited by stratification. In comparison with the Richardson number flux, turbulent kinetic energy production, P , as defined in Equation 7 is also calculated and its time averaged (1 minute) values are plotted in Figure 6 (b). Production, which is calculated using the product of velocity fluctuations –also called Reynolds stresses– is a good indicator about the turbulent kinetic energy observed at the water column and in general, it reached its peak values at the water withdrawal level. This shows the effects of water withdrawal during the measurement period. A more detailed discussion of this effect is provided in the modeling section. Buoyancy flux, B , is plotted Figure 6 (c) and this figure shows that Buoyancy flux is most effective at 9 meters depth between 30 to 50 minutes after the initiation of the monitoring campaign. By definition, buoyancy flux is sensitive to fluctuations in temperature data and Figure 5 provides evidence to fluctuations in temperature data as recorded by the bottom sensors (located at 9 meters).

5. REFORMULATION OF STOKES' SETTLING VELOCITY

Stokes' settling velocities were calculated using fluid properties derived from observed temperatures. Elçi *et al.* (2009) and Elçi, (2008) discussed sampling of the sediments of Tahtali Reservoir bottom and the water column. Based on these studies, mean diameter of the sediment is assumed as 0.068 mm and sediment density is assumed as 1.65 kg/m³ in the calculations. Figure 7 shows the settling velocities calculated based on temperature measurements observed at 30 minutes and 90 minutes after the initiation of the measurement campaign. As provided in Equation 11, velocities calculated by the Stokes' formulation show strong dependence on the density and viscosity distribution in the water column which are both functions of temperature data (Equation 6 and

7). However vertical velocities recorded by the ADCP which is an indicator of how the scatterers in the water move in vertical showed completely different pattern than those predicted using Stokes' formulation (Figure 8). Using the turbulence characteristics discussed in the earlier section, the authors investigated whether modification of the estimated Stokes' settling velocities would be possible using these turbulence characteristics to match the observed vertical velocities.

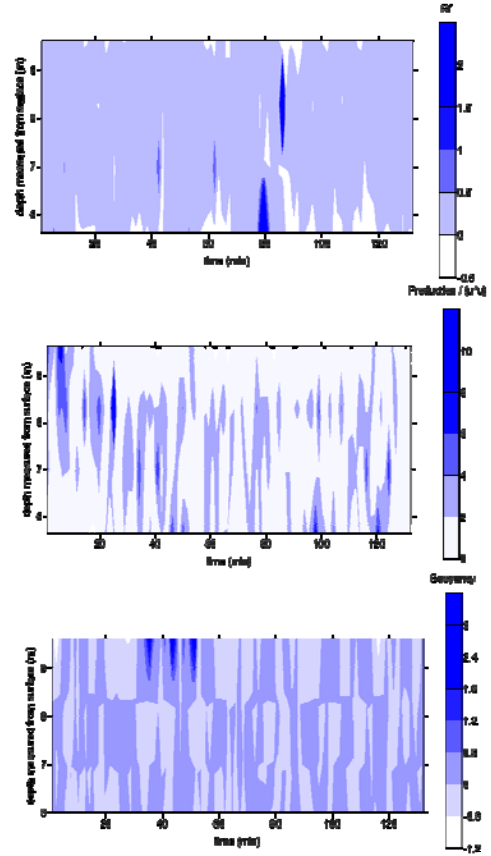


Fig. 6 Time averaged (1 minute) values of the Richardson number flux, R_f , (a) turbulent kinetic energy production, P , (b) Buoyancy flux, B , (c) during the measurement period.

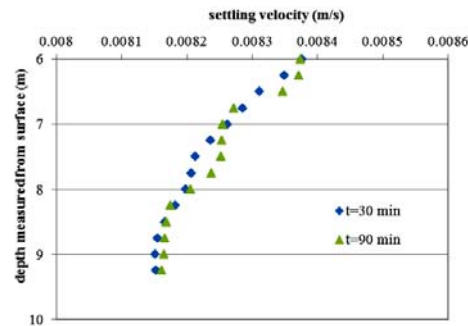


Fig. 7. Variation of settling velocity as calculated by the Stokes' formulation at 30 and 90 minutes after the initiation of the measurement campaign.

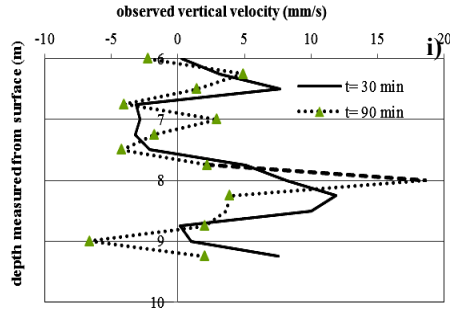


Fig. 8. Variation of the vertical velocity as monitored by the ADCP at 30 and 90 minutes after the initiation of the measurement campaign.

ii) Modification of Stokes' settling velocity for turbulent flow was achieved through use of turbulence characteristics. Vertical velocity profiles estimated by Stokes' formulation based on monitored temperature data were multiplied by Richardson flux, Buoyancy flux, Production and nondimensionalized Reynolds stresses. Among these parameters multiplication of the vertical velocities by the (nondimensionalized Reynolds stresses) $(\overline{u'w'})/w^2$ gave the best results (Figure 9). Comparisons of monitored and estimated settling velocities time series was assessed by the root-mean-square error (RMSE) and RMSE were calculated as 0.0015 and 0.0020 m/s corresponding to 12% and 17% of the monitored maximum vertical velocity at the corresponding profiles.

It was also observed that, when production of turbulence was high, modified settling velocities matched the monitored velocities better. So; it was concluded that modification of Stokes' settling velocities by turbulent kinetic energy production profiles performs better for high turbulent conditions. The methodology also needs to be further improved for different stratification and inflow/outflow conditions.

6. NUMERICAL MODELING OF FLOW IN THE WITHDRAWAL ZONE

6.1 Computational Mesh

In order to construct the mesh, the geometry to be modeled is defined as 100 m long, 200 m wide water column having 30 meters of depth (Figure 10). The intake structure is defined through a 2 m diameter fluid pipe and 9 meters below the surface (second outlet from the surface) having a length of 200 m positioned at the middle of one side. Meshing of the model domain was achieved using sweep method enabling definition of smaller cell sizes (0.3 m) close to the intake and increase of cell size as departed in the vertical to the water surface. Meshing of the model domain by this method shortened the simulation time considerably. Time step is taken as 0.25 s; number of time steps is selected as 40 and maximum number of iterations is

selected as 20 in the simulations.

6.2 Parameters, Boundary and Initial Conditions

Side walls are defined as symmetry and velocity inlet (0.5 m/s and 1 m/s corresponding 1.5 and 3 m³/s of discharge) is applied to simulate the withdrawal in the model. Water density is assumed to depend only temperature, thus a formula describing the relationship between the water density and temperature (Equation 6) is specified by a user defined function (UDF) in C language and this function is input into FLUENT. The temperature profile given in Figure 2 is input as initial condition using Define/User-define/Function/Interpreted steps in the model.

6.3 Comparison to Theoretical Velocity Distribution in the Withdrawal Layer

Previous literature on selective withdrawal mainly included the lowering of upper water layer (drawdown) and focused on defining a critical discharge at which the drawdown occurs (Wood 2001) and on predicting the thickness of the horizontal layer at the level of the intake (Ivey and Blake, 1985). However, literature on describing theoretical velocity distribution in the withdrawal layer is very limited. Based on experimental data Bohan and Grace (1973) obtained the following equation:

$$v = \frac{u}{u_{\max}} = \left(1 - \frac{h}{H} \frac{\Delta\rho'}{\Delta\rho_{\max}} \right)^2 \quad (10)$$

This equation considers the density gradient, and if the density distribution is linear it obtains a symmetrical shape with respect to the orifice center. If the density gradient is larger at one side (above or below the orifice), maximum velocity is observed at that side according to this equation. Comparison of numerical model results with the theoretical dimensionless velocities calculated for the simulated profile (Figure 11) showed that simulated

velocities were in a better agreement (RMSE: 0.2 u/umax) for x/H=1, where x is the horizontal distance measured from the orifice and H is the total depth of the water column. Also, in the simulations maximum velocities were observed above the orifice and reached to 0.13 m/s (Figure 12). In fact, depth at which maximum velocities are observed increased as the observation point approached to the intake, whereas velocities calculated by the theoretical velocity distribution did not show such a withdrawal pattern.

6.4 Simulation of Flow Using Different Turbulence Models

For simulations of maximum velocities, turbulence models performed pretty much the same as it is observed further away from the intake (Figure 13). At the intake, however, maximum withdrawal velocity for k-omega turbulence model was less than the other two turbulence models (k-epsilon and Reynolds) those gave the similar velocity values (RMSE=0.03 m/s).

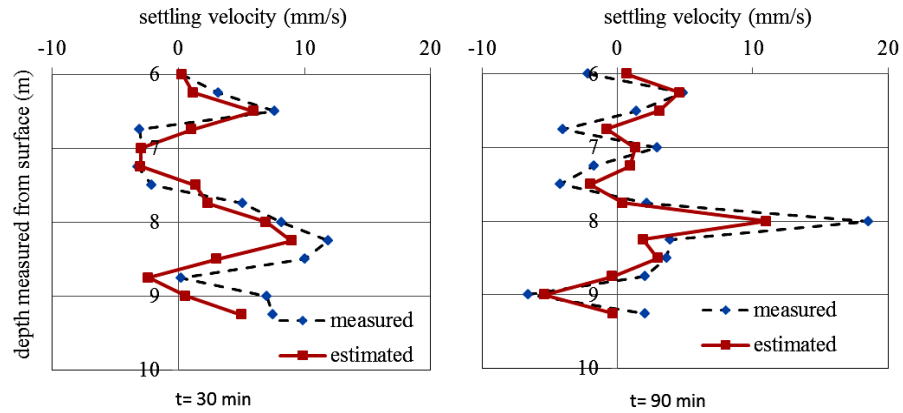


Fig. 9. Comparison of the measured vertical velocities with the modified settling velocities estimated by the Stokes' equation.

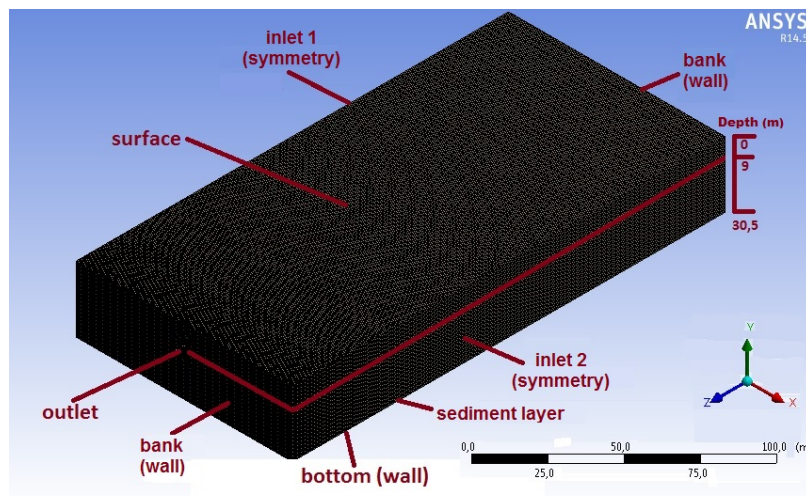


Fig. 10. Computational mesh used in the simulations.

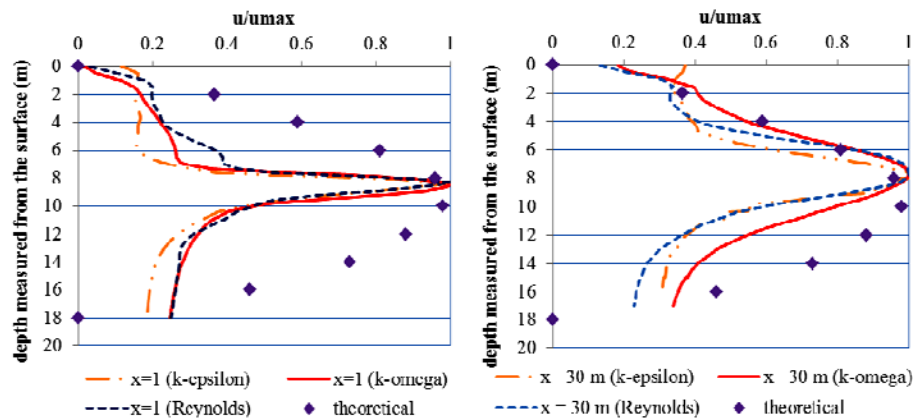


Fig. 11. Comparison of nondimensional velocities for different turbulence models with the theoretical equation defined based on experimental data Bohan and Grace (1973).

Velocities were also compared at different distances ($X = 0, 1, 2, 4, 10, 20$ and 30 m) from the intake (Figure 14). Results of the simulations indicated a drawdown of the location of observed maximum velocities (from 6.9 to 8.8 m of depth measured

from the surface) at all simulations. Drawdowns in each case were formulized through linear equations and the best match was obtained for the k-epsilon turbulence model ($R^2 = 0.97$).

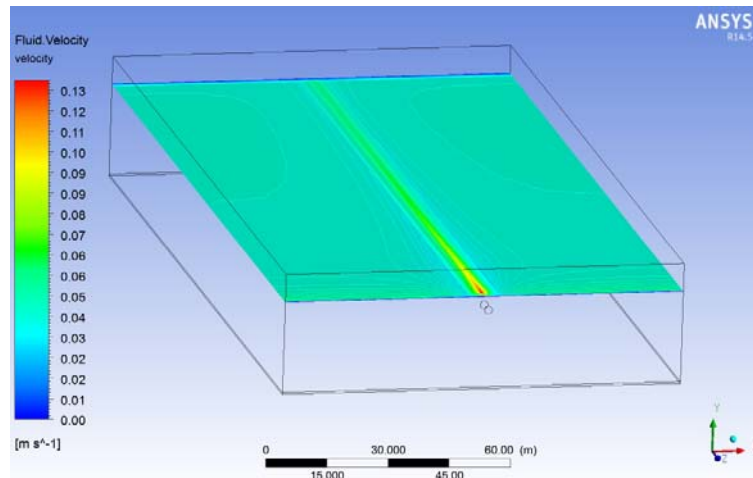


Fig. 12. Modeled velocities at 7 meters below the water surface using $k-\epsilon$ turbulence model.

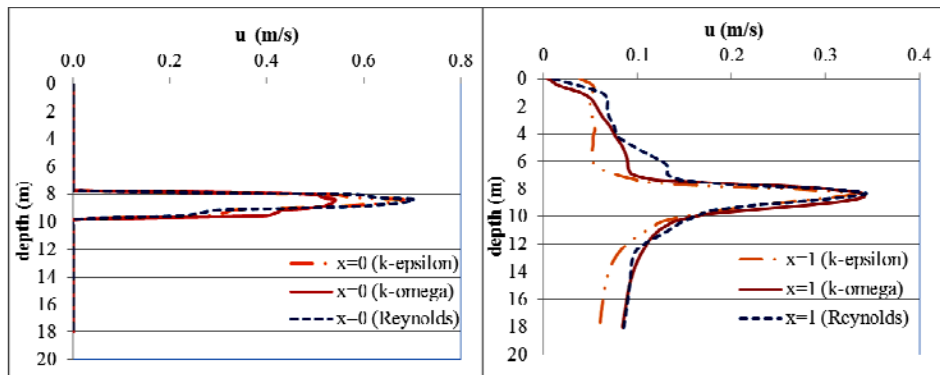


Fig. 13 Comparison of velocities simulated using different turbulence models at the intake and 1 m distance to the intake.

Velocities were also compared at different distances ($X=0, 1, 2, 4, 10, 20$ and 30 m) from the intake (Figure 14). Results of the simulations indicated a drawdown of the location of observed maximum velocities (from 6.9 to 8.8 m of depth measured from the surface) at all simulations. Drawdowns in each case were formulated through linear equations and the best match was obtained for the $k-\epsilon$ turbulence model ($R^2=0.97$).

To investigate the dynamics behind these results further, turbulent kinetic energy values nondimensionalized by maximum velocities were also calculated for the different turbulence models close to the intake structure. Calculated turbulent kinetic energy values at the intake were again slightly different ($RMSE=1.4 \times 10^{-7}$) for $k-\epsilon$ and Reynolds turbulence models but were much less than turbulent kinetic energy values calculated by the $k-\omega$ model (Figure 15). Since $k-\omega$ turbulence model showed discrepancy from the other two models for prediction of flow velocity and turbulent kinetic energy at the intake, this discrepancy was attributed to the different wall treatments in the turbulence models. As discussed earlier, standard wall functions are applied for $k-\epsilon$ turbulence model and Reynolds stress models in these simulations, since these models are valid only

far from solid boundaries. The $k-\omega$ model at the other hand solves the transport equations all the way to the wall through use of fine mesh. Turbulent kinetic energy values are also plotted at the intake to include for the lateral distances ($Y=47-53$ m). Figure 16 and Figure 17 show the difference of nondimensionalized turbulent kinetic energy values simulated by $k-\epsilon$ and Reynolds models and $k-\epsilon$ and $k-\omega$ models respectively. Figure 17 showed that turbulent kinetic energy values simulated by the $k-\omega$ model were much higher at the level of orifice. A pear shape difference was observed between the $k-\omega$ and $k-\epsilon$ models where the maximum difference was reached at 8.3 m depth measured from the surface. As discussed earlier, standard wall function is utilized for $k-\epsilon$ and Reynolds turbulence models.

6.5 Effects of Different Wall Treatment Functions on Simulations

Next, flow velocities and turbulent kinetic energy were simulated by $k-\epsilon$ turbulence model utilizing three different wall functions to investigate further the effects of wall functions on the results. Although different wall treatment functions do not have significant effects on the flow velocities, nonequilibrium wall treatment gives lower turbulent

kinetic energy values than standard and two layer wall treatments outside the intake region as shown in Figure 18. All three wall treatments predicted the same turbulent kinetic energy values along the orifice (8-10 m). More dissipation in turbulent kinetic energy predicted by the nonequilibrium wall functions is related to the logarithmic velocity profile modified to include pressure gradient. Different than the other wall functions using near wall velocity profiles, nonequilibrium wall functions use the modified logarithmic velocity profile to enable better prediction of adverse pressure gradient flows and separation.

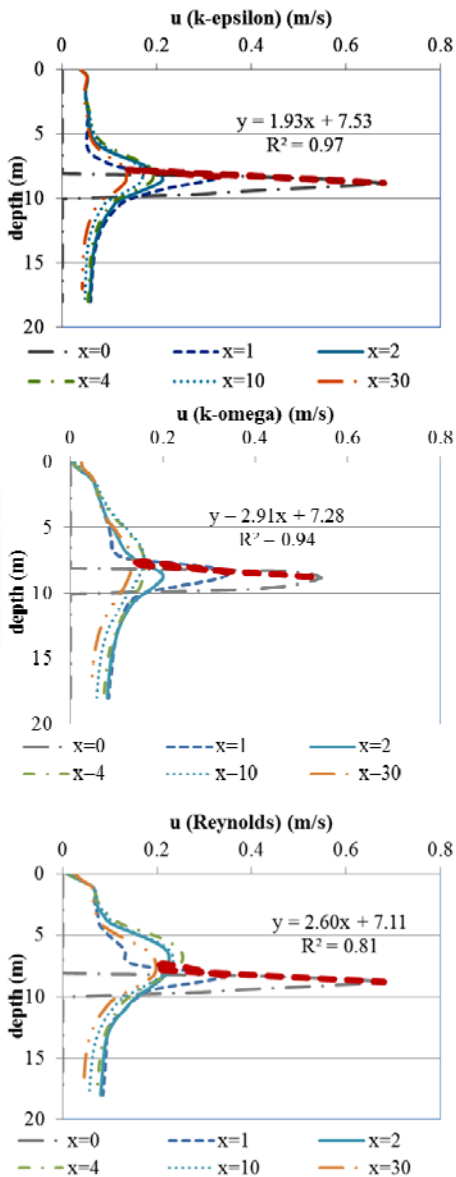


Fig. 14. Comparison of velocities simulated using different turbulence models at different locations to the intake (standard wall function is utilized in k-epsilon model and RE models).

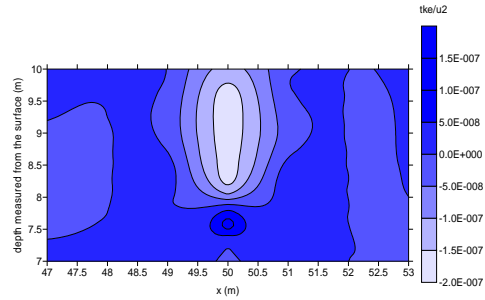


Fig. 16 Difference of nondimensionalized turbulent kinetic energy values simulated by k-epsilon and Reynolds models (standard wall function) at the intake.

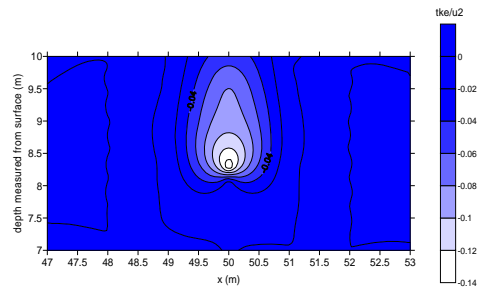


Fig. 17 Difference of nondimensionalized turbulent kinetic energy values simulated by k-epsilon (standard wall function) and k-omega models at the intake.

6.6 Comparison of Results Simulated via Two Different k- ω Models

As mentioned earlier within the text, the k- ω model solves the transport equations all the way to the wall through use of fine mesh. A wall treatment function thus is not incorporated to the model. FLUENT however, provides options between standard and shear-stress transport (SST) k- ω models. Comparison of velocities at the intake simulated by two different k- ω models did not yield a significant difference, but comparison of nondimensionalized turbulence kinetic energy showed that The SST model predicted much lower turbulence kinetic energy than the standard k- ω model. The maximum predicted values (tke/u^2) at the center of the orifice decreased from 0.16 to 10^{-4} whereas these values were about 10^{-6} for the other two turbulence models. The SST model incorporates a modified turbulent viscosity to account for the transport of the turbulent shear stress and this difference is attributed to this modification.

7. CONCLUSIONS

Advances in measurement technologies enabled monitoring of detailed temperature and velocity profiles from where turbulence characteristics of the flow can be examined. Based on the data obtained from the field deployment conducted in June 2013, the flow characteristics of Lake Tahtali could be examined for the deployment period. Following the

previous studies, turbulence characteristics were defined through two commonly used parameters: buoyancy flux and Richardson number flux.

Richardson number flux during the deployment period indicated values greater than 0.25, indicating that turbulent mixing is strongly inhibited by stratification. When turbulent kinetic energy production values were calculated and plotted however we could observe high production intervals coinciding with lower values of Richardson number flux. Although both turbulence kinetic energy production and dissipation were observed along the water column, dissipation was more dominant close to the bottom which was explained by the bottom friction.

Through the use of the acoustic Doppler velocity profiler we could directly measure the particle velocities rather than estimating indirectly from the balance of settling and diffusive flux gradients. Monitored vertical particle velocities were assumed equal to the settling velocity of the particles present in the water column. Then these velocities were compared to the Stokes' settling velocities modified by turbulent characteristics.

As for the reformulation of the Stokes' settling velocity, modification of the velocities by the turbulent kinetic energy production profiles worked better than the modification of the velocities by the Richardson number flux. Even modification with the nondimensionalized Reynolds stresses ($(\overline{u'w'})/w^2$) alone lead to nice vertical profiles although the velocity intensities were not in the same magnitude. It was also observed that, when production of turbulence was high, modified settling velocities matched the monitored velocities better. So; it was concluded that modification of Stokes' settling velocities by turbulent kinetic energy production profiles performs better for high turbulent conditions. We can infer from these results that vertical transport of momentum by turbulence can be quantified and used to modify settling velocities provided for the laminar flow. However; it should be also noted that, the methodology needs to be further improved for different stratification and inflow/outflow conditions.

In the second part of the paper, simulation of flow near the intake using different turbulence models were discussed. Results of the simulations indicated a drawdown of the location of observed maximum velocities (from 6.9 to 8.8 m of depth measured from the surface) at all simulations. Drawdowns in each case were formulated through linear equations and the best match was obtained for the k-epsilon turbulence model ($R^2=0.97$). The dynamics behind these results were investigated further via plots of turbulent kinetic energy values nondimensionalized by maximum velocities. Turbulent kinetic energy values simulated by the k-omega model were much higher at the level of orifice that the other two turbulence models. This difference was attributed to the use of standard wall functions in k-epsilon turbulence model and Reynolds stress models

whereas the k-omega model solves the transport equations all the way to the wall.

Next, flow velocities and turbulent kinetic energy were simulated to investigate the effects of different wall functions. Although different wall treatment functions did not have significant effects on the flow velocities, nonequilibrium wall treatment gave lower turbulent kinetic energy values than standard and two layer wall treatments outside the intake region. More dissipation in turbulent kinetic energy predicted by the nonequilibrium wall functions was related to the logarithmic velocity profile modified to include pressure gradient.

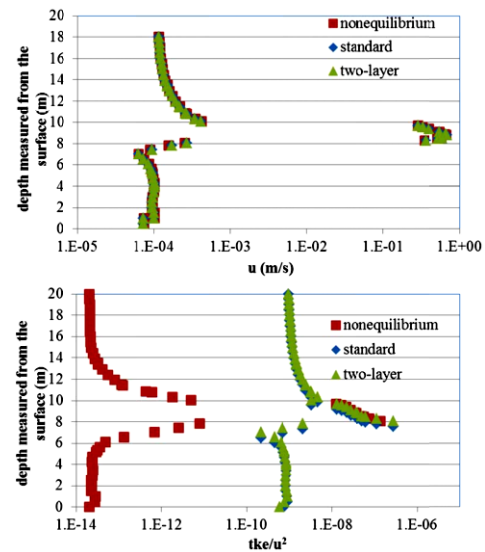


Fig. 18. Comparison of measured velocity and nondimensionalized turbulence kinetic energy at the intake for different wall functions used in the k-epsilon model.

Finally, comparison of two different k-omega models were provided in the paper. Although comparison of velocities did not yield a significant difference, comparison of nondimensionalized turbulence kinetic energy showed that the SST model predicted much lower turbulence kinetic energy than the standard k-omega model. This difference was related to modified turbulent viscosity utilized in the SST k-omega model.

As a result of this study, it can be concluded that use of different turbulence models did not have significant effects especially if the interest is on the flow hydrodynamics away from the intake structure ($x/h < 1$ (x : distance to the intake; h : depth of the water column)). By the intake structure however, utilization of different turbulence models had significant effects especially on turbulence kinetic energy production. Thus, when modeling withdrawal flow, either use of SST k-omega models solving equations all the way to the wall or k-epsilon models with the nonequilibrium wall function of which logarithmic velocity profile is modified to include the pressure gradient is recommended.

ACKNOWLEDGEMENT

This study is financially supported by Izmir Institute of Technology Research Fund (project no: IYTE-2012-03) and Turkish Science and Technological Research Council (TUBITAK) through the 114M019 project. We also would like to thank to the staff of Izmir Water and Sewage Authority (IZSU) for their contributions during collection of the data.

REFERENCES

- Bohan, J. P. and J. L. Grace, Selective Withdrawal From Man-Made Lakes, Technical Report.
- Burchard, H., P. D. Craig, J. R. Gemmrich, H. Van Haren, P. P. Mathieu, H. E. M. Meier, W. A. M. Nimmo Smith, H. Prandke, T. P. Rippeth, E. D. Skillingstad, W. D. Smyth, D. J. S. Welsh and H. W. Wijesekera (2008). Observational and numerical modeling methods for quantifying coastal ocean turbulence and mixing. *Progress in Oceanography* 76(4), 399–442.
- Caliskan, A. and Ş. Elçi (2009). Investigation of the hydrodynamics and withdrawal effects in a stratified lake. *Water Resources Management* (23), 1257-1273.
- Elçi, Ş. (2008). Effects of thermal stratification and mixing on reservoir water quality. *Limnology* 9(2), 111-123.
- Elçi, Ş., R. Aydın and P. A. Work (2009). Estimation of suspended sediment concentration in rivers using acoustic methods. *Environmental Monitoring and Assessment by Springer* (159), 255-265.
- Etemad-Shahidi, A. and J. Imberger (2001). Anatomy of turbulence in thermally stratified lakes, *Limnology Oceanography* 46(5), 1158-1165.
- Geyer, W. R., M. E. Scully and D. K. Ralston (2008). Quantifying vertical mixing in estuaries. *Environmental Fluid Mechanics* 8, 495-509.
- H-73-4, U. S. Army Engineer Waterways Experiment Station, March 1973.
- Ivey, G. N. and J. Imberger (1991). On the nature of turbulence in a stratified fluid, part 1: the energetics of mixing. *J. Phys. Oceanogr.* 21, 650–658.
- Ivey, G. N. and S. Blake (1985). Axisymmetric withdrawal and inflow in a density-stratified container. *Journal of Fluid Mechanics* 161(1), 115-137.
- Ivey, G. N., K. B. Winters and J. R. Koseff (2008). Density stratification, turbulence, but how much mixing *Annu.Rev.Fluid Mechanics* 40, 169-184.
- Kawanisi, K. and R. Shiozaki (2008). Turbulent Effects on the Settling Velocity of Suspended Sediment. *J. of Hydraulic Engineering* 134, 261-266.
- McCutcheon, S. C., J. L. Martin, T. O. J. R. Barnwell (1993). *Water Quality in Maiment*, DR (Editor). Handbook of Hydrology, McGraw-Hill, New York, NY.
- Saggio, A. and J. Imberger (2001). Mixing and turbulent fluxes in the metalimnion of a stratified lake. *Limnology and Oceanography* 46(2), 392-409.
- Stacey, M. T., S. G. Monismith and J. R. Burau (1999). Observations of turbulence in a partially stratified estuary. *J. Phys. Oceanog.* 29, 1950-1970.
- Wood, I. R. (2001). Extensions to the theory of selective withdrawal. *Journal of Fluid Mechanics* 448(1), 315-333.
- Yang, C. T. (1996). *Sediment transport: Theory and practice*, McGraw- Hill, New York.